

# 1 **Root exudation facilitates water infiltration and rewetting of dry soil**

2 Emma Gomez Peral<sup>a</sup>, Andrew Mair<sup>a</sup>, Iker Martin Sanchez<sup>a</sup>, Gloria de las Heras  
3 Martinez<sup>a</sup>, Mariya Ptashnyk<sup>b</sup>, Lionel X Dupuy<sup>a c †</sup>

4 <sup>a</sup> Department of Conservation of Natural Resources, Neiker, Derio, 48160,  
5 Spain

6 <sup>b</sup> Department of Mathematics, School of Mathematical and Computer Sciences,  
7 Heriot-Watt University, Scotland, United Kingdom

8 <sup>c</sup> Ikerbasque, Basque Foundation for Science, Bilbao, 48009, Spain

9 <sup>†</sup> Corresponding author: [ldupuy@neiker.eus](mailto:ldupuy@neiker.eus)

## 10 **Keywords**

11 Root architecture, exudates, water infiltration, drought

## 12 **Abstract**

13 The way plant roots facilitate water infiltration in soil may be just as important as  
14 the efficiency with which the root system in turn extracts it from the soil. Here  
15 we studied the mechanisms through which the root system facilitates water  
16 infiltration through a dry soil layer. Dye tracing experiments were conducted in  
17 model soil microcosms to characterise how root growth and exudation affects  
18 the permeability of dry layers of the model soil. Results showed that dissolved  
19 root exudates may be the primary facilitator of water infiltration, which may be  
20 linked to water surface tension. We conclude that in dry soil, root architecture  
21 and root exudation may combine to facilitate the infiltration of water and  
22 decrease the water lost by evaporation. These findings could enhance our  
23 understanding of the traits that provide drought resistance in crops.

## 24 **Introduction**

25 Hydrologists have long acknowledged the significant role of vegetation in  
26 influencing water movement in soil, and as Clothier and Green aptly expressed,  
27 the roots are the "big movers" (Clothier and Green 1997). A primary driver is the  
28 extraction of water from the soil through root uptake and subsequent  
29 transpiration, which not only reduces soil water content but also causes water to  
30 move along gradients of the water potential. However, prior to uptake, the roots  
31 also influence water transport through modifications of the soil hydraulic  
32 properties. The presence of plant roots in soil has been linked to preferential  
33 flow of water in dye-tracing experiments. For example, Jačka et al. (2021)  
34 observed increased dye concentration around plant roots in a tracer  
35 experiment. This finding was corroborated by measurements of saturated  
36 hydraulic conductivity in soil column experiments, which showed that the soil  
37 conductivity increased due to the presence of roots (Leung et al. 2018). Various  
38 studies have also demonstrated that the hydraulic conductivity increases with  
39 the root length density (Xiao et al. 2024). In field experiments, it was also  
40 observed that most types of vegetation increase the infiltration rate of bare soil  
41 (Marshall et al. 2014; Song et al. 2017).

42 Changes in soil hydraulic properties can be attributed to physical modifications  
43 in the soil's pore structure. As roots grow, they displace the surrounding soil,  
44 creating a cavity and rearranging the distribution of the surrounding soil pores  
45 (Dexter 1987). Because the size and connectivity of soil pores determine the  
46 resistance of the flow of water, these changes in soil porosity in turn affect the  
47 permeability of the soil (Schulz et al. 2019). In the study of (Anselmucci et al.  
48 2021) roots grown in sand created an increase in porosity because of dilation.  
49 In more structured soil however, the expansion of the root cavity compacted the  
50 surrounding soil, and this can lead to a reduction in the soil porosity (Bruand et  
51 al. 1996; Helliwell et al. 2017; Koebernick et al. 2019), although this usually  
52 occurs in the bulk soils which initial porosity is low (Lucas et al. 2019). Other  
53 factors such as the shrinking or decay of the root can also create macropores  
54 (Ni et al. 2019; Duddek et al. 2022) where the flow of water can occur with least  
55 resistance.

56 Chemical modifications of the soil solution caused by rhizodeposition can  
57 influence water movement in soils as well. High molecular weight polymers  
58 such as mucilage increase the viscosity of the soil solution (Read et al. 1999)  
59 which in turns reduces the flow speed and increases the resistance to water  
60 movements. Mucilages behave as hydrogels because they contain polymers  
61 that are hydrophilic, crosslinked, and possess the ability to absorb and retain a  
62 significant amount of water (Naveed et al. 2019). This property is critical to  
63 maintain moisture around the root when the soil is drying (Carminati et al.  
64 2010). Once dry however, root rhizodeposits can become water repellent and  
65 may slow down water infiltration during rewetting (Ahmed et al. 2016).  
66 Rhizodeposits also contain surfactants, and this likely facilitates water  
67 movement during infiltration and the rewetting of dry and water repellent soils  
68 (Read et al. 1999, 2003).

69 This study aims to determine whether physical or chemical modifications of the  
70 soil substrate have a greater impact on soil water infiltration. We carried out dye  
71 tracing experiments in model transparent soil microcosms containing dry  
72 hydrophobic layers and combined image analysis and mathematical models to  
73 quantify the respective role of root exudation and root growth on the  
74 permeability of the dry transparent soil layer.

## 75 **Material and methods**

### 76 *Plant material and germination*

77 Seeds of winter wheat (*Triticum aestivum* var. *Filon*) were first hydrated for one  
78 hour in sterilised water and then sterilised for 15 minutes in a 1% calcium  
79 hypochlorite solution (042548.30, Thermo Scientific, Spain). After numerous  
80 washes, seeds were placed in distilled water for two more hours before transfer  
81 to agar plates in an incubator at 23 °C. The incubation time was three days  
82 when running microcosm experiments and five days for root exudate extraction  
83 experiments.

### 84 *Extraction of root exudates*

85 Seedlings whose radicles had reached 3-5 cm were placed on a 3D printed  
86 punched plate (5 mm diameter holes arranged on a regular grid with 2 cm  
87 spacing). Each plate hosted approximately 50 seeds and was placed on top of a  
88 15x21x7 glass dish (Ikea, Spain) with roots dipping into 1 L of Hoagland  
89 nutrient solution (092621822, MP Biomedicals, Spain) adjusted to a pH of 7  
90 using potassium hydroxide (KOH). Plants grew in a growth chamber (23 °C,  
91 60% humidity with 14/10 h day/night cycle) with the nutrient solution aerated  
92 using a pneumatic pump (Souslow, Spain) during seven days. To suppress the  
93 growth of contaminants and avoid root responses to light, the glass dish was  
94 painted in black on the outside. After six days of growth, the nutrient solution  
95 was replaced with 0.5 L of sterile distilled water. Roots grew 24 h in distilled  
96 water before three 50 ml falcon tubes (EP0030122232, Sigma-Aldrich, Spain)  
97 were used to collect 120 mL of solution from each glass dish. The root exudate  
98 solutions were then frozen at -80 °C. To adjust the concentration of root  
99 exudates, falcon tubes containing root exudate solutions were freeze-dried and  
100 2 mL of distilled water were subsequently added before pooling all the root  
101 exudates from one glass dish into a 15 mL falcon tube (EP0030122194, Sigma-  
102 Aldrich, Spain). The root exudate solution obtained was freeze-dried a second  
103 time for weighing, and distilled water was added to adjust the concentration of  
104 the root exudate solution to 1 mg mL<sup>-1</sup>. Root exudates were then stored frozen  
105 at -20 °C. We ran 4 experiments with a total of 8 plates.

#### 106 *Transparent soil*

107 Transparent soil was prepared as described earlier (Downie et al. 2012). Briefly  
108 Nafion pellets (NR50 1100, Ion Power Inc, USA) were fractured to a texture  
109 similar to sand (0.25 to 1.25 mm) using a freezer mill (6850 Freezer/Mill, SPEX  
110 CertiPrep, UK) and a series of sieves. The pH of the substrate was then  
111 adjusted by washing with Hoagland nutrient solution. With a density for Nafion  
112 of approximately 1.9 g cm<sup>-3</sup> and a porosity of 0.3, the estimated substrate  
113 density is 1.58 g cm<sup>-3</sup>.

#### 114 *Microcosm preparation*

115 Microcosm chambers were assembled following the protocol described by Liu et  
116 al. (2025) from microscope glass slides (76 × 26 × 1 mm<sup>3</sup>, VWR, Spain). Glass  
117 slides were bonded by 4 mm polydimethylsiloxane spacer (PDMS, SYLGARD  
118 184, Sigma-Aldrich, Spain) following surface treatment by oxygen plasma for 15  
119 s at 100 W (HPT-100, Henniker Plasma, UK). After surface treatment, the glass  
120 and PDMS surfaces were brought together, and pressure was applied to ensure  
121 a strong bond between all surfaces in contact. Following the assembly of the  
122 different part, the space available for placing plants and soil is 68 × 18 × 4 mm<sup>3</sup>.  
123 The microcosm was then filled with transparent soil layers with different water  
124 content (Figure 1A). The bottom 1.5 cm layer (approximate dry weight of 1.7 g)  
125 of the microcosm chamber was filled with transparent soil fully saturated with  
126 water. Then a 0.8 cm layer of dry transparent soil was added (approximate dry  
127 weight of 0.9 g). The dry transparent soil was obtained by heating in an oven at

128 105 °C for 24 hours. The top layer was 1 cm thick (approximate dry weight of  
129 1.1 g) of transparent soil fully saturated with water.

### 130 *Dye tracing experiment*

131 First, we studied how the presence of plant roots affected the permeability of  
132 the dry transparent soil layer. Control samples consisted of microcosm  
133 chambers prepared as described in the previous section but without seedlings  
134 transferred into them. Wheat seedlings were transferred when the root length  
135 was 0.5 to 0.8 mm in length. All microcosm chambers were closed with parafilm  
136 tape (HS234526B, Sigma-Aldrich, Spain) and placed in a growth chamber at 23  
137 °C, 60% humidity with 14/10 h day/night cycle. Distilled water was added to the  
138 samples using a syringe to maintain the top layer of transparent soil saturated.  
139 The tracer dye was added 8 days after the transfer of the root seedlings. Most  
140 plants had at least one root in the bottom of the microcosm chamber at that  
141 time. A food dye (red food colorant, Vahiné, Spain) was diluted to 0.1 mL mL<sup>-1</sup> to  
142 obtain the tracer dye solution. 0.2 mL of that solution was then added on the top  
143 of the microcosm chamber. Half an hour later, the first image was taken (t=0  
144 hour). The following images were taken 24, 48 and 72 hours after the first  
145 image. The experiment was repeated 3 times with a total of 15 samples with  
146 roots and 13 controls samples without roots. Two root samples were discarded  
147 because of leakage of the microcosm chamber.

148 In the second experiment, we quantified the effect of root exudates on the  
149 infiltration of water. In this case the tracer dye solution was diluted with the root  
150 exudate solution so that resulting root exudate concentration was approximately  
151 0.9 mg mL. Then 0.2 mL of that solution was then added at the top of the  
152 microcosm (concentration of root exudate approximately 0.16 mg g<sup>-1</sup>). All  
153 microcosm chambers were sealed with parafilm tape and placed in the growth  
154 chamber under the previously described conditions. The first images were  
155 obtained half an hour after inoculation (t=0 hour). The following images were  
156 obtained 72, 96 and 120 hours after the first image. The experiment was  
157 repeated 3 times with a total of 19 samples containing root exudates and 16  
158 control samples containing only water. One control sample was discarded due  
159 to a leak.

160 In a third experiment, we studied the effect of the presence of root exudates in  
161 the dry transparent soil layer. To prepare dry transparent soil containing root  
162 exudates, 5 g of wet transparent soil was mixed 1 mL of the root exudate  
163 solution. The wet transparent soil was then left to dry at 105 °C for 48 hours in  
164 an oven. Therefore, the resulting root exudate concentration in the dry  
165 transparent soil was similar to that of the top layer, 0.633 mg g<sup>-1</sup>. Four types of  
166 samples were prepared. Namely, samples that did not contain root exudates  
167 (NN), samples that contained root exudates in the middle layer (NE), samples  
168 that contained root exudates in the top layer (EN), and samples that contained  
169 root exudates in both layers (EE). All microcosm chambers were sealed with  
170 parafilm tape and placed in the growth chamber. The first image was acquired  
171 half an hour after introduction of the tracer dye (t=0 hour). The following images

172 were taken 72, 96 and 120 hours after the first image. The experiment was  
173 repeated 3 times with a total of 8 samples for each combination.

174 Finally, in the fourth experiment, we studied the effect of the rearrangement of  
175 transparent soil particles induced by penetration of the dry middle layer. A  
176 hypodermic needle (12684536, Fisher Scientific, Spain) was pushed  
177 approximately 2.5 cm into the transparent soil. The needle was 0.8 mm in  
178 diameter which is similar to the diameter of wheat roots (Hallam et al. 2021).  
179 Control samples were not penetrated by the hypodermic needle. 0.2 ml of the  
180 tracer dye solution was added at the top of the microcosm chamber. All  
181 microcosm chambers were sealed with parafilm tape and placed in the growth  
182 chamber. Half an hour after inoculation of the tracer dye, the first image was  
183 taken ( $t=0$  hour). The following images were taken 24, 48 and 120 hours after  
184 the first image. The experiment was repeated 3 times with a total of 15 samples  
185 and 15 controls. One sample was discarded due to a leak.

### 186 *Quantitative image analysis*

187 Images of microcosm chambers were acquired using a Canon EOS 2000D  
188 camera (Canon, Spain) with an exposure time of 1/1000 s, ISO-400 speed, and  
189 focal length was 39 mm and a f-stop of f/5.6. Colour images were stored  
190 uncompressed in colour format (sRGB) at resolution of 6000 × 4000 pixels. To  
191 quantify the tracer dye concentration from image data, calibration samples with  
192 dye concentration of 0, 0.01, 0.05, 0.1, 0.5 and 1 mL mL<sup>-1</sup> were prepared in  
193 triplicate. Images were acquired for each sample and relationships were  
194 established between the dye concentration and the image brightness, and  
195 between dye concentration and the image saturation value (Figure 1B). To  
196 quantify dye concentration in the microcosm chambers containing transparent  
197 soil layers, regions of the image corresponding to the top, middle and bottom  
198 layers of transparent soil were cropped from the raw image data. Images were  
199 transformed to hue, saturation and brightness (HSB) format and the saturation  
200 value was used to determine the dye concentration (Figure 1C). All image  
201 processing tasks were performed using the ImageJ software (Schmid et al.  
202 2010).

203 The permeability of the dry transparent soil layer  $k$  [s<sup>-1</sup>] was calculated using the  
204 following formula

205

$$k = \frac{(C_2 - C_1) / (C_0 - C_1)}{T_1 - T_0} \quad (1)$$

206 Here,  $C_0$  and  $C_1$  are the dye concentrations at time  $T_0$  in the top and bottom  
207 layer respectively.  $C_2$  is the dye concentration in the bottom layer at time  $T_1$ .

### 208 *Statistical analysis*

209 Statistical models were constructed to analyse the effects of plant roots, root  
210 exudates or to analyse the effect of the needle on both the permeability  $k$  and  
211 the tracer dye concentration in the dry transparent soil layer. We used  
212 generalized linear models to correlate the permeability of the dry transparent

213 soil layer with both time and treatment effects. We tried different variance  
 214 functions and found that heterogeneity was best corrected using variance  
 215 covarying with treatments rather than with time. Model selection was based on  
 216 the Akaike information criterion (AIC). Statistical analyses were performed with  
 217 R (R Core Team 2021) using the glm package.

### 218 *Model of water infiltration and rewetting*

219 Water transport in the transparent soil microcosms was represented using the  
 220 model of Mair (unpublished). The model solves Richards equations (Richards,  
 221 1931), on a spatial domain which here is in 1D,  $x \in [-3.3, 0]$ ,  $t \in (0, T]$ . Final  
 222 time was  $T=5$  days (120 hours).

223 To match the experimental conditions, the pressure head was adjusted to -0.01  
 224 kPa -0.1 cm at the top -100 kPa in the middle layer and -0.01 kPa at the  
 225 bottom. The water content and hydraulic conductivity functions were expressed  
 226 from the soil pressure head using the formulations of (van Genuchten 1980)  
 227 and (Mualem 1976):

$$\theta(h, c_W, c_D) = \theta_r + (\theta_s - \theta_r) S_e(h, c_W, c_D), \quad (2)$$

$$S_e(h, c_W, c_D) = \frac{1}{(1 + |\alpha(c_W, c_D) h|^n)^m}, \quad (3)$$

$$K(h, c_W, c_D) = K^* + \alpha_K K_s K_r(h, c_W, c_D).$$

228 Both the Nafion particles and root exudates are known to have different  
 229 behaviour during wetting and drying (hysteresis in both the hydraulic  
 230 conductivity and water retention functions), and this was modelled represented  
 231 using the model of Kool and Parker (1987) for water content  $\theta$  ( $\text{cm}^3 \text{cm}^{-3}$ ) and  
 232 the model of Vogel and Zhang (1996) for the hydraulic conductivity  $K$  ( $\text{cm d}^{-1}$ ).  
 233 Hence, we focused primarily on the influence of the concentration of root  
 234 exudates suspended in the solution  $c_W$  ( $\text{mg mL}^{-1}$ ) and the concentration of root  
 235 exudates dried and attached to the surface of the particles  $c_D$  ( $\text{mg g}^{-1}$ ). These  
 236 parameters affect the inverse air entry pressure head  $\alpha$  ( $\text{cm}^{-1}$ ), as described in  
 237 (Karagunduz et al. 2001), through the surface tension of water  $\gamma$  ( $\text{mN m}^{-1}$ ) and  
 238 water contact angle  $\omega$  (rad)

$$\alpha^W = \alpha_0^W \times \frac{\gamma(c_W)}{\gamma_0} \times \frac{\cos(\omega_0)}{\cos(\omega(c_D))}, \quad (4)$$

$$\alpha^D = \alpha_0^D \times \frac{\gamma_0}{\gamma(c_W)},$$

239 Here  $\alpha^W$  and  $\alpha^D$  are the inverse air entry pressure head for wetting and drying  
 240 respectively and  $\alpha_0^W$  and  $\alpha_0^D$  are the default inverse air entry pressures if no  
 241 exudates are present in either form. The effect of root exudates is also  
 242 incorporated into the saturated hydraulic conductivity as

$$K_s^Z(c_W, c_D) = K_{s,0}^Z \times \left( \frac{\gamma_0}{\gamma(c_W)} \right)^\beta \times \frac{\cos(\omega(c_D))}{\cos(\omega_0)}, \quad (5)$$

243 where  $Z = W, D$  for wetting or drying. Here  $K_{s,0}^Z$  are the default saturated  
 244 hydraulic conductivities during wetting and drying if no exudates are present,

245 and  $\beta$  determines the extent to which an exudate-induced reduction in surface  
 246 tension increases hydraulic conductivity. The terms  $K^*$  and  $\alpha_K$  in (3) are  
 247 included to effectively incorporate hysteresis. The expressions for surface  
 248 tension and contact angle as functions of the concentrations of suspended and  
 249 dried root exudates are fitted to the data of Read et al. (2003) and Zickenrott et  
 250 al., (2016) respectively,

$$\gamma(c_W) = 47.5 + \frac{72.86 - 47.5}{(1 + e^{18.79(c_W - 0.36)})}, \quad (6)$$

$$\omega(c_D) = \frac{3.529}{18} \pi (1 + e^{-1879.14c_D})^{-4.39}.$$

251 The dynamics of the root exudates in solution and the dried root exudates are  
 252 given by the following differential equations

$$\partial_t(\theta c_W) - \partial_x(\theta D_W \partial_x c_W - \vec{q} c_W) = \rho \kappa_W c_D - \theta \kappa_D c_W, \quad (7)$$

$$\rho \partial_t c_D = \theta \kappa_D c_W - \rho \kappa_W c_D,$$

253 where  $D_W$  ( $\text{cm}^2 \text{d}^{-1}$ ) is the coefficient of diffusion of root exudates through soil  
 254 water,  $\vec{q}$  ( $\text{cmd}^{-1}$ ) is the advective flux of soil water and  $\rho$  ( $\text{mg cm}^{-3}$ ) is the bulk  
 255 density of Nafion. The terms  $\kappa_W$  and  $\kappa_D$  ( $\text{d}^{-1}$ ) are the rates at which dried root  
 256 exudate joins the soil water solution and root exudate in solution dries to the  
 257 pore surface respectively. Finally, the movement of dye within the chambers is  
 258 modelled using an additional differential equation

$$\partial_t(\theta u) - \partial_x(\theta D_u \partial_x u - \vec{q} u) = 0. \quad (8)$$

259 Here  $u$  ( $\text{mL mL}^{-1}$ ) is the concentration of dye in solution and  $D_u$  ( $\text{cm}^2 \text{d}^{-1}$ ) is the  
 260 diffusion coefficient of the dye in solution. The dye concentration at the start of  
 261 the experiment is  $0.04 \text{ mL mL}^{-1}$  in the upper layer where root exudates have  
 262 been introduced, 0 otherwise.

263 A finite element scheme, with an implicit Euler discretisation in time, was used  
 264 to approximate solutions to the coupled system of equations.

### 265 *Model parameterisation*

266 Model parameters were taken from previously published literature assuming  
 267 that coarse sand would be the best approximation of the transparent soil.  
 268 However, the reference inverse air-entry pressure heads  $\alpha_0^D, \alpha_0^W$  and saturated  
 269 hydraulic conductivities  $K_{s,0}^D, K_{s,0}^W$  were altered considerably from the values cited  
 270 in the literature in order to reflect the hydrophobicity of dry Nafion that was  
 271 observed in the control infiltration experiments. The full list of parameters can  
 272 be found in Table 1.

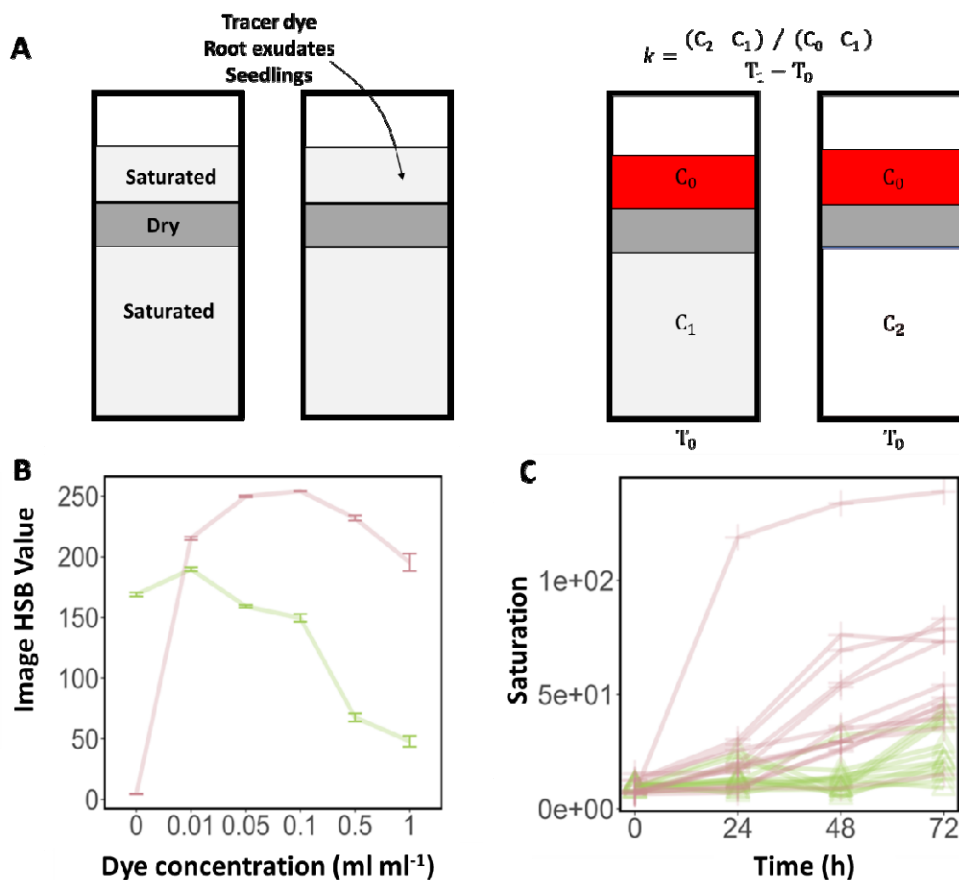
<i>Parameter</i>	<i>Value</i>	<i>Source</i>
$\theta_{r,0}$	$1 \times 10^{-10} \text{ cm}^3 \text{cm}^{-3}$	$N \setminus A$
$\theta_{s,0}$	$0.404 \text{ cm}^3 \text{cm}^{-3}$	(Benson et al. 2014)
$\alpha_0^D$	$0.049 \text{ cm}^{-1}$	(Benson et al. 2014)

$\alpha_0^W$	0.164 cm <sup>-1</sup>	(Benson et al. 2014)
$n$	3.16	(Benson et al. 2014)
$m$	0.684	(Benson et al. 2014)
$K_{s,0}^D$	$8.196 \times 10^{-4}$ cm d <sup>-1</sup>	(Carsel and Parrish 1988)
$K_{s,0}^W$	$4.917 \times 10^{-4}$ cm d <sup>-1</sup>	(Carsel and Parrish 1988)
$D_W$	0.65 cm <sup>2</sup> d <sup>-1</sup>	(Scott et al. 1995), average taken
$\rho$	1.9 g cm <sup>-3</sup>	(Oberbroeckling et al. 2002)
$D_u$	0.5 cm <sup>2</sup> d <sup>-1</sup>	(Syms 2017)

273 Table 1: Model parameter values derived from the scientific literature

274 Two types of critical parameters could not be determined from the literature.  
275 First, the coefficient linking surface tension to hydraulic conductivity  $\beta$  is both  
276 very specific to the model system and could not be found in the literature. To  
277 calibrate the value of  $\beta$ , data was used from the second experiment and  
278 compared observations to simulated dye concentration between depths  $-3.3$  cm  
279 and  $-1.8$ cm at times  $t = 3, 4, 5$  d. Using Bayesian optimisation (Brochu et al.  
280 2010) we obtained the values  $\beta$  that most accurately matched experimental  
281 results. The rates at which root exudates dissolve or reverse to a dry state are  
282 also very specific to our model system and were obtained in a similar way. Here  
283 we used the observation from the third experiment and Bayesian optimisation to  
284 determine the values of  $\kappa_W$  and  $\kappa_D$  that best predicted dye concentrations in the  
285 lower third of the domain.

286



287

288 **Figure 1:** Model system for quantifying the impact of root exudates on water transport  
 289 (A) Diagram of the microcosm system. At the start of the experiment, the microcosm is comprised of three layers of transparent soil (left). The top  
 290 layer of transparent soil is saturated with water to allow fast diffusion of the dye. The middle layer is oven dried to produce a hydrophobic barrier. The bottom  
 291 layer is saturated with water for precise determination of the quantity of dye moving through the dry layer. During the experiment (right) the dye was  
 292 introduced at  $T_0$  at the top of the microcosm chamber and diffused rapidly through the top layer of transparent soil. At time  $T_1$  the tracer dye became  
 293 visible, and a permeability coefficient could be calculated. (B) The dye concentration in the liquid can be quantified from the image saturation value  
 294 (red) at low dye concentration, and with the image brightness value (green) at high concentration. (C) Example of time lapse data of the saturation value  
 295 captured in the bottom transparent soil layer.

## 302 Results

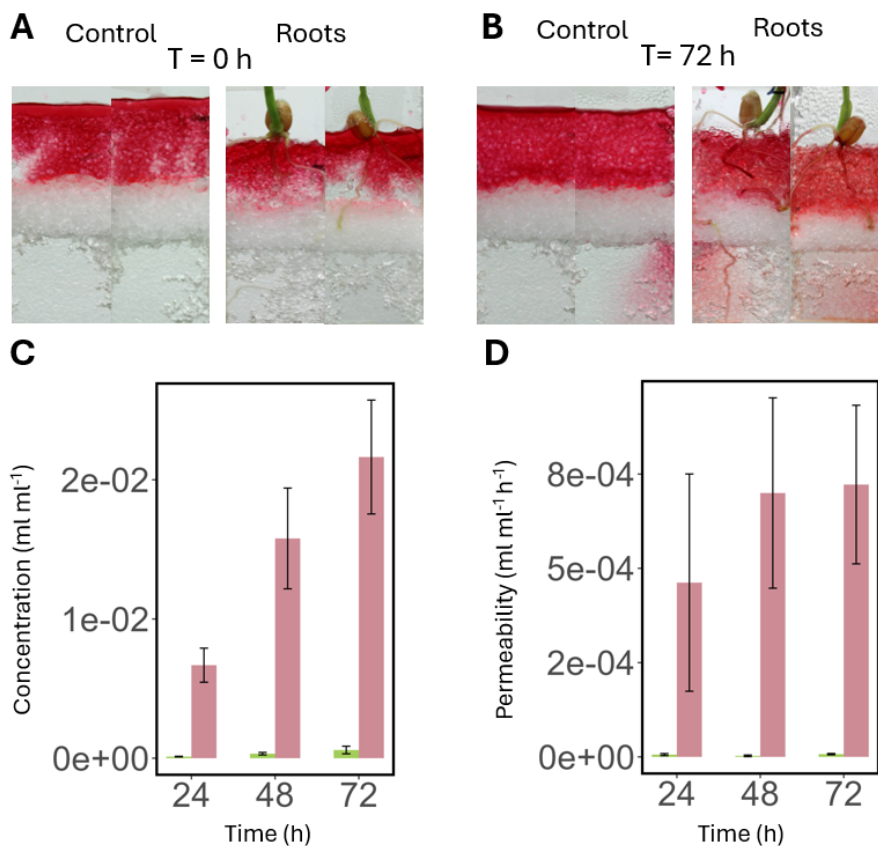
303 *Plant roots increase the infiltration of water through dry transparent soil in a*  
 304 *microcosm system*

305 Following introduction into the microcosm, the dye was observed spreading non  
 306 homogeneously but rapidly within the top transparent soil layer (Figure 2A), but  
 307 there was no evidence of the dye being absorbed by the particles. The dry

308 transparent soil layer blocked further spreading of the tracer dye into the lower  
309 layers of transparent soil. There was no obvious effect of the roots on the  
310 transport of the dye at this stage of the experiment. The spatial distribution of  
311 the tracer dye was analysed over a 72-hour period following the start of the  
312 experiment (Figure 2B). In the control samples, the wetting front advanced  
313 downward by 1 to 2 mm during the first 48 hours. We did not observe further  
314 progress of the wetting front during the rest of the experiment, even in the case  
315 where the tracer dye was seen in the bottom transparent soil layer (Figure 2B).  
316 24 hours after the introduction of the tracer dye, no coloration was observed in  
317 the bottom transparent soil layer of the control samples. Only 5 samples out of  
318 13 showed some coloration at the end of the experiment. In the samples  
319 containing roots, we observed a greater movement of the wetting front. 48  
320 hours after the experiment began, the wetting front had advanced downward by  
321 3 to 4 mm. When the root was visible, we observed the dye both attached to the  
322 root and in the surrounding transparent soil (Figure 2B). The tracer dye began  
323 to appear in the lower transparent soil layer 24 hours after the introduction of  
324 the tracer dye. The coloration increased in intensity over time until the end of  
325 the experiments. All samples showed some coloration at the end of the  
326 experiment.

327 The quantitative analysis of the image data confirmed visual observations. The  
328 dye concentration in the dry transparent soil layer increased with time (Figure  
329 2C). In the case of the control samples, the dye concentration increased up to a  
330 mean value of  $3.5 \times 10^{-4}$  mL mL<sup>-1</sup>. In the case of the samples containing plants,  
331 an increase in dye concentration was observed during the entire experiment  
332 with a final dye concentration recorded at  $2.1 \times 10^{-2}$  mL mL<sup>-1</sup>. Quantitatively, the  
333 estimated dye concentration in the dry transparent soil layer increased when a  
334 root was present, but not in control treatments (Figure 2C). We did not measure  
335 a significant change over time in the permeability of the dry transparent soil  
336 layer in the control samples (Figure 2D). Statistical analysis of the data using a  
337 linear model showed that in the absence of the root, the permeability of the dry  
338 transparent soil layer was not significantly different from 0 during the entire  
339 experiment ( $p=0.23$  and  $p=0.69$  for slope and intercept). However, the presence  
340 of the root had a significant effect on the rate of increase in the permeability of  
341 the dry transparent soil layer ( $p<0.001$ ).

342



343

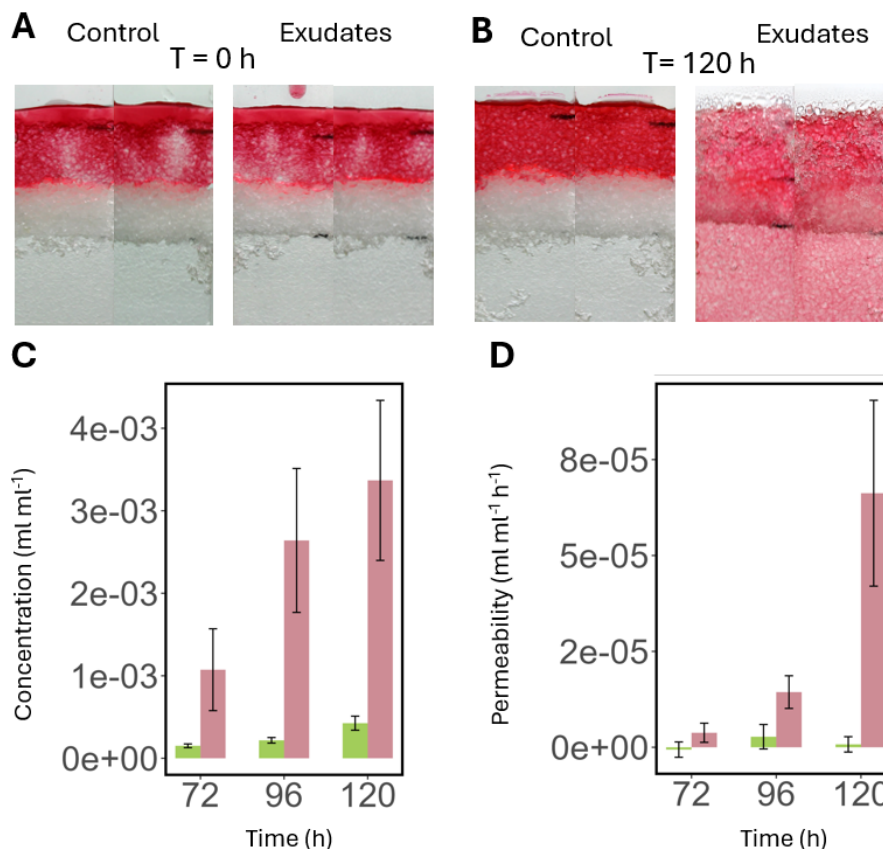
344

345 **Figure 2:** Effect of the presence of winter wheat (*Triticum aestivum*) roots on the  
346 infiltration of a tracer dye through a dry transparent soil layer. **(A)** Microcosm  
347 samples just after introduction of the tracer dye into the top transparent soil  
348 layer. Sample without root (Control, left) and sample with root (right). **(B)**  
349 Microcosm samples 72 hours after introduction of the tracer dye. **(C)**  
350 Concentration of the tracer dye in the dry transparent soil layer measured at  
351 different time points. **(D)** Permeability of the dry transparent soil layer measured  
352 at different time points. C&D, Green control samples and pink samples with  
353 roots.

354 *Root exudates increase water infiltration through the dry transparent soil layer*

355 Following introduction into the microcosm, the dye was observed spreading non  
356 homogeneously but rapidly within the top transparent soil layer (Figure 3A), but  
357 there was no evidence of the dye being absorbed by the transparent soil  
358 particles. The dry transparent soil layer blocked further spreading of the tracer  
359 dye into the lower layers of transparent soil. There was no obvious effect of the  
360 presence of root exudates on the transport of the dye at this stage of the  
361 experiment. The spatial distribution of the tracer dye was analysed over a 120-  
362 hour period following the start of the experiment (Figure 3A&B). In control  
363 samples, the wetting front did not advance during the first 72 hours but had  
364 advanced by 1-2 mm by the end of the experiment (Figure 3A&B). 96 hours  
365 after the introduction of the tracer dye, red coloration began visible in the bottom

366 transparent soil layer in all samples. The coloration increased in intensity with  
367 time until the end of the experiments. In the samples with root exudates, the  
368 wetting front advanced irregularly but continuously into the dry layer throughout  
369 the experiment. At the end of the experiment, the dry transparent soil layer was  
370 completely wet (Figure 3A&B).



371

372 **Figure 3:** Effect of the presence or absence of root exudates from winter wheat  
373 (*Triticum aestivum*) on the infiltration of a tracer dye through a dry transparent soil  
374 layer. (A) Microcosm samples just after introduction of the tracer dye into the top  
375 transparent soil layer. Sample without root exudates (left) and sample with root  
376 exudates (right). (B) Microcosm samples 120 hours after introduction the tracer  
377 dye. (C) Concentration of the tracer dye in the dry soil layer measured at  
378 different time points. (D) Permeability of the dry transparent soil layer measured  
379 at different time points. C&D green control samples and pink samples with  
380 exudates.

381

382 Quantitatively, the mean dye concentration in the dry transparent soil layer  
383 increased with time (Figure 3C) for both control samples and samples  
384 containing root exudates. When samples contained root exudates, the increase  
385 in dye concentration in the bottom layer was sustained during the experiment.  
386 We did not measure a significant change with time in the permeability of the dry  
387 transparent soil layer in the control samples (Figure 3D). For samples with root  
388 exudates, permeability was maximal 120 hours after introduction of the tracer

389 dye. Statistical analysis of the data using a linear model showed that in the  
390 absence of root exudates, the permeability of the dry transparent soil layer was  
391 not significantly different from 0 during the entire experiment ( $p=0.54$  and  
392  $p=0.45$  for slope and intercept). However, the presence of root exudates had a  
393 significant effect on the rate of increase in the permeability of the dry  
394 transparent soil layer ( $p<0.001$ ).

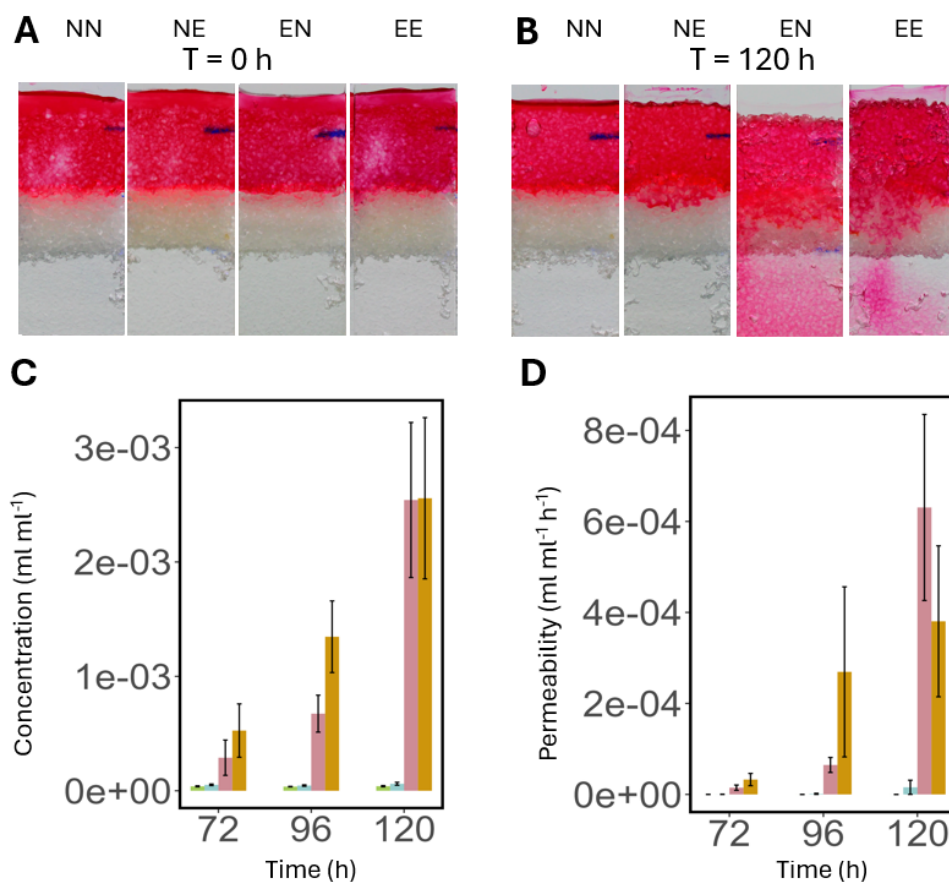
395 *The presence of root exudates in the dry layers has limited effect on water*  
396 *infiltration and rewetting of the dry transparent soil layer*

397 Following introduction into the microcosm, the dye spread following a similar  
398 pattern as reported in the previous experiments (Figure 4A). There was no  
399 obvious effect of the presence of root exudates (in the top or dry layer) on the  
400 transport of the dye at this stage of the experiment. The spatial distribution of  
401 the tracer dye was analysed over a 120-hour period following the start of the  
402 experiment (Figure 4A&B). In samples, that did not contain root exudates, the  
403 wetting front did not advance during the first 72 hours but had advanced by 1 to  
404 1.5 mm both in the NN treatment and in the NE treatments (Figure 3A&B). 96  
405 hours after the introduction of the tracer dye, red coloration began visible in the  
406 bottom transparent soil layer in all samples. The coloration increased in  
407 intensity with time until the end of the experiments. No colouration was  
408 observed at the bottom of the microcosm chambers at any stage of the  
409 experiment. There were no strong visual differences between samples with and  
410 without root exudates in the dry transparent soil layer. Samples containing root  
411 exudates in the tracer dye (EN and EE) exhibited qualitatively similar behaviour  
412 to samples containing root exudates in the tracer dye in experiment 2.

413 Quantitative analysis of the image data confirmed the visual observations. The  
414 dye concentration in the dry transparent soil layer increased with time (Figure  
415 4C). For samples containing no exudates in the tracer dye, the increase was  
416 gradual, but for samples containing root exudates in the tracer dye, a sharp  
417 increase in dye concentration was observed within the first 72 hours and this  
418 was followed by a more moderate increase in dye concentration. We did not  
419 measure a significant change over time in the permeability of the dry  
420 transparent soil layer in samples containing water in the tracer dye (Figure 4D).  
421 In the case of samples with root exudates in the top layer, permeability steadily  
422 increased during the experiment. Statistical analysis of the data using a linear  
423 model showed that in the absence of root exudates, the permeability of the dry  
424 transparent soil layer was not significantly different from 0 during the entire  
425 experiment but the presence of root exudates in the top transparent soil layer  
426 had both a significant effect on the slope and intercept of the relationship  
427 ( $p<0.001$  and  $p=0.01$  respectively). The presence of root exudates in the middle  
428 layer did not have a significant effect on the permeability of the dry transparent  
429 soil layer.

430

431



432

433 **Figure 4** Effect of location of root exudates of winter wheat (*Triticum aestivum*) on  
434 the infiltration of a tracer dye through a dry transparent soil layer. (A) Microcosm  
435 samples just after introduction of the tracer dye into the top transparent soil  
436 layer. (B) Microcosm samples 120 hours after the start of the experiment. (C)  
437 Concentration of the tracer dye in the dry transparent soil layer measured at  
438 different time points. (D) Permeability of the dry transparent soil layer measured  
439 at different time points. In C&D green NN, blue NE pink EN and yellow EE.

440 *Physical modifications due to penetration of the dry transparent soil layer do not*  
441 *affect the infiltration and rewetting*

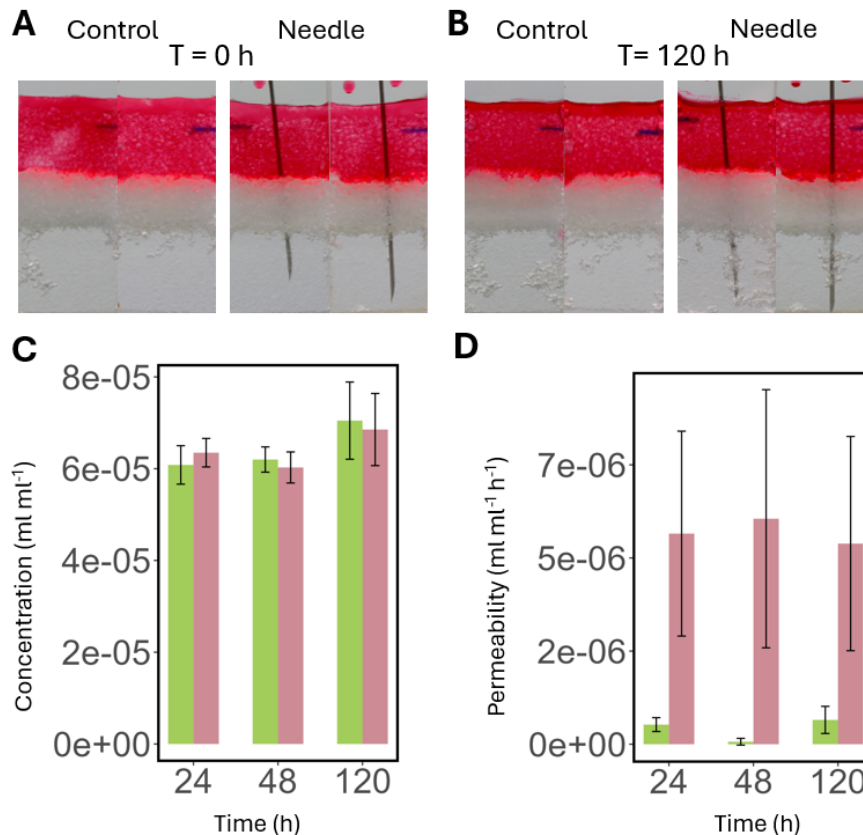
442 Following introduction into the microcosm, the dye spread following a similar  
443 pattern than experiments where the tracer dye did not contain root exudates  
444 (Figure 5A&B). There was no obvious effect of the presence of the needle on  
445 the transport of the dye at this stage of the experiment. The spatial distribution  
446 of the tracer dye was analysed over a 120-hour period following the start of the  
447 experiment. No difference was observed between treatments during the entire  
448 experiment. No dye was observed at the bottom transparent soil layer, nor in  
449 the dry transparent soil layer. At the end of the experiment, we observed that  
450 the wetting front had advanced about 1 mm downward for all treatments.

451 Quantitative analysis of the image data confirmed the visual observations. The  
452 dye concentration in the dry transparent soil layer did not increase with time in

453 both conditions (Figure 5C). Calculation of the permeabilities of the dry  
454 transparent soil layer revealed that that when the needle was present, there  
455 was much higher variability and mean value for the permeability (Figure 5D),  
456 which is likely due to the needle having an effect on the saturation of the image.  
457 Statistical analyses however showed that the presence of a needle did not have  
458 an effect on the calculated permeability ( $P = 0.0073$ ).

459

460



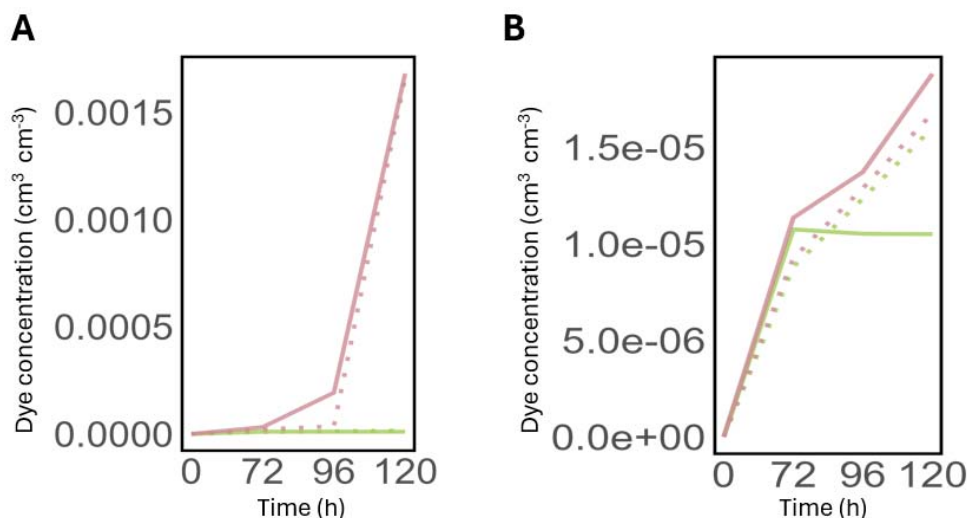
461

462

463 **Figure 5** Effect of the presence or absence of a needle on the infiltration of a  
464 tracer dye through a dry transparent soil layer. (A) Microcosm samples just after  
465 introduction of the tracer dye into the top transparent soil layer. Sample without  
466 needle (Control, left) and sample with needle (right). (B) Microcosm samples  
467 120 hours after introduction of the tracer dye. (C) Concentration of the tracer  
468 dye in the dry transparent soil layer measured at different time points. (D)  
469 Permeability of the dry transparent soil layer measured at different time points.  
470 C&D, green control samples, pink samples with a needle.

471 *The hydraulic conductivity is critically sensitive to surface tension and root*  
472 *exudate concentration*

473 Model calibration completed successfully with optimal parameters values for  
474  $\beta^*$ ,  $\kappa_D^*$ ,  $\kappa_W^*$  determined from experimental data. Following calibration, the  
475 predicted dye concentration was plotted against experimental data (Figure 6).  
476 Results showed good agreements between the model and experimental  
477 observations. Discrepancies were observed in the control treatment where no  
478 exudates were introduced (NN). Experiments showed an abrupt stop in the  
479 permeability of the dry transparent soil layer, which the model could not  
480 represent. The estimated model parameters gave also interesting insights into  
481 the effects of root exudates on water transport in transparent soil. The exponent  
482 of the power law relating surface tension to hydraulic conductivity was  $\beta = 8.8$ ,  
483 indicating that the concentration of root exudate in solution had a strong effect  
484 on the hydraulic conductivity of transparent soil. The parameter for the  
485 solubilisation or sorption of root exudates  $\kappa_D^* = 9.9 \times 10^{-2} d^{-1}$  and  $\kappa_W^* = 1.8 \times$   
486  $10^{-2} d^{-1}$  also provided useful insight. They showed that although the rate of  
487 solubilisation may not be limiting, because permeability is very small at the start  
488 of the experiments, the fraction of the transparent soil exposed to water limits  
489 the capacity of the dry root exudates to meaningfully increase the infiltration of  
490 water.



491

492 **Figure 6** Model predictions against experimental data for dye concentration in  
493 the bottom transparent soil layer. (A) Comparison between model and  
494 experimental data for experiments when root exudates are introduced in the top  
495 layer in the tracer dye solution. EN is shown in pink and NN is shown in green.  
496 (B) Comparison between model and experimental data for experiments when  
497 root exudates are introduced dry in the middle layer. NE is shown in pink and  
498 NN is shown in green. In all plots, dotted lines represent model predictions data  
499 whereas plain lines indicate experimental observations.

## 500 Discussion

501 *Water infiltration and loss of water from the rhizosphere*

502 Plant roots absorb water stored in the soil's pore spaces, which is subsequently  
503 replenished through irrigation, rainfall, or capillary rise. However, a substantial  
504 portion of the water input is lost before it can be absorbed by the plant. Losses  
505 are due to evaporation, deep percolation, runoff, and lateral flow and can be  
506 particularly high before canopy closure (Chen et al. 2020). In a cropping  
507 system, 20% of the evapotranspiration is typically due to bare soil evaporation,  
508 but it can exceed 50% of the total influx of water. For example, a review of the  
509 seasonal losses of water by evaporation in rain fed wheat in Australia showed  
510 that between 27% and 68% of the evapotranspiration is due to evaporation  
511 (Unkovich et al. 2018). The percentage of evaporation was between 15% and  
512 40% in Maize in a range of water and N regimes (Hernández et al. 2015). In  
513 sandy soils, deep percolation can become the dominant source of water loss.  
514 Nassah et al. (2018) reported nearly 50% loss of water inputs lost due to water  
515 leaving the rooted zone through deep percolation.

516 The root system architecture, the spatial and topological arrangement of roots  
517 into a soil, is therefore a critical trait to determine the ability of a crop to extract  
518 water from the soil. First because it determines the regions of the soil where  
519 water can be extracted. When a root system is shallow, the plant can more  
520 readily acquire immobile nutrients that are strongly absorbed to soil particles  
521 (Lynch and Brown 2002). When the root system is deep, it can reach the water  
522 table and extract groundwater during drought (Lynch 2013). However, water  
523 balance in soil is very dynamic and another important role of root systems may  
524 be to intercept water, that is to distribute water into soil following a rainfall, to  
525 minimize losses from the rhizosphere. Although roots are known to facilitate  
526 preferential water flow through the soil, this function of root systems has been  
527 largely overlooked as a valuable trait to improve water management in cropping  
528 systems. Recently, mathematical models that combined water uptake with  
529 preferential flow induced by plant roots showed that root system architectures  
530 may have very different abilities to intercept rainfall water, and that root system  
531 ideotypes may vary as a function of soil type (Mair et al. 2023).

532 The experiments described in this study aimed to investigate the impact of root  
533 traits on water infiltration in dry soil. We used a dye tracing approach rather than  
534 infiltrometers to miniaturise and shorten the duration of the microcosm  
535 experiments. Observation of the dye also gave insights into the mechanisms of  
536 infiltration. The use of an artificial soil improved the accuracy of measurements  
537 since all the dye below the dry layer was considered in the measurement of the  
538 fluxes. The artificial soils also made experiments more manageable. Nafion<sup>TM</sup>,  
539 the material used as substrate, is mildly hydrophobic when dry (water contact  
540 angle of 105° (Goswami et al. 2008)), and resulted in low infiltration rates but  
541 with measurable effects after a few days of experiments. Agricultural soils which  
542 have low organic matter content usually exhibit higher infiltration rates (Basset  
543 et al. 2023), and organic matter rich soils such as peat are too hydrophobic  
544 when dry (water contact angle of up to 120° (Valat et al. 1991)).

545 *Physical processes involved in preferential flow induced by plant roots*

546 We observed that root exudation was a primary factor influencing the infiltration  
547 of water through dry soil. This result suggests that surfactants found in root  
548 exudates may play a crucial role in affecting water movement within the soil.  
549 Not only root exudates are known to contain surfactants (Read et al. 2003), but  
550 measurements of water retention in rhizosphere and bulk soil have also  
551 indicated that rhizosphere solutions may exhibit lower surface tension (Whalley  
552 et al. 2005). Surfactants are also used for the irrigation of plants growing in  
553 hydrophobic soils and arid environments (Baratella and Trinchera 2018;  
554 Ogunmokun et al. 2020), which confirms that the exudation of surfactants may  
555 be a beneficial trait in certain soils.

556 Experiments using syringe needles indicated that changes in porosity induced  
557 by root growth may not affect significantly the infiltration of water. In a coarse  
558 and loosely packed, sand, similar to our artificial soil, root growth was shown to  
559 induce dilation of <4% and increase the porosity of about 10% over a layer of  
560 <2 mm around the root (Anselmucci et al. 2021). The Kozeny–Carman equation  
561  $K \propto \text{porosity}^3 / (1 - \text{porosity})^2$  predicts that such changes can result in an  
562 increase of 50% of the hydraulic conductivity (Schulz et al. 2019). But a 1 mm  
563 thick layer represents about 10% of the cross section of the soil. Also, dilation of  
564 the rhizosphere soil is associated with reduction of porosity further away from  
565 the root and collectively, this would likely limit the changes in the hydraulic  
566 conductivity to less than 5%. In the Young-Laplace equation, pore size and  
567 surface tension exert equal effects on capillary entry pressure (Hallett 2008).  
568 Given that root exudates have been shown to reduce surface tension by 27%,  
569 reducing it from 72 mN m<sup>-1</sup> to 50 mN m<sup>-1</sup> (Read et al. 2003), it is plausible for  
570 root exudation to have a stronger effect than dilation in some conditions.

#### 571 *Root exudation as a mechanism to influence water availability in soil*

572 During drought conditions, evidence suggests that both the quantity and  
573 composition of root exudates undergo significant changes (Karlowsky et al.  
574 2018; Williams and de Vries 2020). However, it remains uncertain whether  
575 these changes reflect a plant's response to modify the physical properties of the  
576 soil. It was suggested that for a large part, changes in root exudation result from  
577 shift in plants metabolic activity, with root exudates reflecting the most abundant  
578 root metabolites (Gargallo-Garriga et al. 2018). The lifespan of root exudates in  
579 soils is likely to be highly variable. Many of the compounds deposited in the soil  
580 by plant roots are consumed by soil microbes (Sasse et al., 2018), and it is  
581 challenging to determine the extent to which changes in soil physical properties  
582 are directly attributable to rhizodeposition, as opposed to being secondary  
583 effects arising from microbial activity. For example, soil bacteria are  
584 extraordinary producers of biosurfactants (Karanth et al. 1999; Domingues et al.  
585 2020). They are also able to synthesize extracellular polymeric substances  
586 (EPS) which enhance soil water retention (Zheng et al. 2018; Benard et al.  
587 2023). The reduction of surface tension typically necessitates small amounts of  
588 a single surfactant molecule, such as Lecithin found in soybeans (Read et al.  
589 2003). Consequently, even subtle changes in the composition of root exudates  
590 could significantly impact soil properties.

591 It is also far from clear what the desired physical properties of the rhizosphere  
592 solution should be. While surfactant production may be desirable in low soil  
593 water content when water is trapped in small pores (Whalley et al. 2005) or in  
594 soils rich in organic matter (strong hysteresis between wetting and drying), the  
595 broader benefits are less clear. The level of organic matter in agricultural soils is  
596 minimal (Loveland and Webb 2003; Rawls et al. 2004) and heterogeneously  
597 distributed (Lehmann et al. 2008). Also, losses due to evaporation and deep  
598 percolation are extremely dependent on rainfall or irrigation patterns. Answering  
599 such questions will be challenging and is likely to require further experimental  
600 characterisation, together with the integration of mathematical modelling and  
601 simulation studies.

## 602 **Acknowledgements**

603 We acknowledge the funding from the Spanish Ministry of Science, Innovation  
604 and Universities under the grant agreements No. PID2020-112950RR-I00 and  
605 No. PID2023-149435OR-I00 (projects MICROCROWD and BIOFLOW). This  
606 work was also supported by the European Union's Horizon Europe under the  
607 grant agreement No.101060124 (Project Root2Res).

608

## 609 **References**

- 610 Ahmed MA, Kroener E, Benard P, et al (2016) Drying of mucilage causes water  
611 repellency in the rhizosphere of maize: measurements and modelling. *Plant Soil*  
612 407:161–171
- 613 Anselmucci F, Andò E, Viggiani G, et al (2021) Imaging local soil kinematics during the  
614 first days of maize root growth in sand. *Sci Rep* 11:22262
- 615 Baratella V, Trinchera A (2018) Organosilicone surfactants as innovative irrigation  
616 adjuvants: Can they improve water use efficiency and nutrient uptake in crop  
617 production? *Agric Water Manag* 204:149–161
- 618 Basset C, Abou Najm M, Ghezzehei T, et al (2023) How does soil structure affect water  
619 infiltration? A meta-data systematic review. *Soil Tillage Res* 226:105577
- 620 Benard P, Bickel S, Kaestner A, et al (2023) Extracellular polymeric substances from  
621 soil-grown bacteria delay evaporative drying. *Adv Water Resour* 172:104364
- 622 Benson CH, Chiang I, Chalermyanont T, Sawangsuriya A (2014) Estimating van  
623 Genuchten parameters  $\alpha$  and  $n$  for clean sands from particle size distribution data.  
624 In: *From soil behavior fundamentals to innovations in geotechnical engineering:*  
625 *Honoring Roy E. Olson.* pp 410–427
- 626 Berry JD, Neeson MJ, Dagastine RR, et al (2015) Measurement of surface and  
627 interfacial tension using pendant drop tensiometry. *J Colloid Interface Sci*  
628 454:226–237
- 629 Brochu E, Cora VM, De Freitas N (2010) A tutorial on Bayesian optimization of  
630 expensive cost functions, with application to active user modeling and hierarchical  
631 reinforcement learning. *arXiv preprint arXiv:10122599*

- 632 Bruand A, Cousin I, Nicoullaud B, et al (1996) Backscattered electron scanning images  
633 of soil porosity for analyzing soil compaction around roots. *Soil Science Society of*  
634 *America Journal* 60:895–901
- 635 Carminati A, Moradi AB, Vetterlein D, et al (2010) Dynamics of soil water content in the  
636 rhizosphere. *Plant Soil* 332:163–176. <https://doi.org/10.1007/s11104-010-0283-8>
- 637 Carsel RF, Parrish RS (1988) Developing joint probability distributions of soil water  
638 retention characteristics. *Water Resour Res* 24:755–769
- 639 Chen S, Du T, Wang S, et al (2020) Evaluation and simulation of spatial variability of  
640 soil property effects on deep percolation and nitrate leaching within a large-scale  
641 field in arid Northwest China. *Science of the Total Environment* 732:139324
- 642 Clothier BE, Green SR (1997) Roots: the big movers of water and chemical in soil. *Soil*  
643 *Sci* 162:534–543
- 644 Dexter AR (1987) Compression of soil around roots. *Plant Soil* 97:401–406
- 645 Domingues VS, de Souza Monteiro A, Júlio ADL, et al (2020) Diversity of metal-  
646 resistant and tensoactive-producing culturable heterotrophic bacteria isolated from  
647 a copper mine in Brazilian Amazonia. *Sci Rep* 10:1–12
- 648 Downie HF, Holden N, Otten W, et al (2012) Transparent Soil for Imaging the  
649 Rhizosphere. *PLoS One* 7:. <https://doi.org/10.1371/journal.pone.0044276>
- 650 Duddek P, Carminati A, Koebernick N, et al (2022) The impact of drought-induced root  
651 and root hair shrinkage on root–soil contact. *Plant Physiol* 189:1232–1236
- 652 Gargallo-Garriga A, Preece C, Sardans J, et al (2018) Root exudate metabolomes  
653 change under drought and show limited capacity for recovery. *Sci Rep* 8:1–15
- 654 Goswami S, Klaus S, Benziger J (2008) Wetting and absorption of water drops on  
655 Nafion films. *Langmuir* 24:8627–8633
- 656 Hallam J, Holden J, Robinson DA, Hodson ME (2021) Effects of winter wheat and  
657 endogeic earthworms on soil physical and hydraulic properties. *Geoderma* 400:.  
658 <https://doi.org/10.1016/j.geoderma.2021.115126>
- 659 Hallett PD (2008) A brief overview of the causes, impacts and amelioration of soil water  
660 repellency—a review. *Soil and Water Research* 3:521–528
- 661 Helliwell JR, Sturrock CJ, Mairhofer S, et al (2017) The emergent rhizosphere: imaging  
662 the development of the porous architecture at the root-soil interface. *Sci Rep*  
663 7:14875
- 664 Hernández M, Echarte L, Della Maggiora A, et al (2015) Maize water use efficiency and  
665 evapotranspiration response to N supply under contrasting soil water availability.  
666 *Field Crops Res* 178:8–15
- 667 Jačka L, Walmsley A, Kovář M, Frouz J (2021) Effects of different tree species on  
668 infiltration and preferential flow in soils developing at a clayey spoil heap.  
669 *Geoderma* 403:115372
- 670 Karagunduz A, Pennell KD, Young MH (2001) Influence of a Nonionic Surfactant on the  
671 Water Retention Properties of Unsaturated Soils. *Soil Science Society of America*  
672 *Journal* 65:1392–1399. <https://doi.org/10.2136/sssaj2001.6551392x>

- 673 Karanth NGK, Deo PG, Veenanadig NK (1999) Microbial production of biosurfactants  
674 and their importance. *Curr Sci* 116–126
- 675 Karlowsky S, Augusti A, Ingrisch J, et al (2018) Drought-induced accumulation of root  
676 exudates supports post-drought recovery of microbes in mountain grassland.  
677 *Front Plant Sci* 9:1593
- 678 Koebernick N, Daly KR, Keyes SD, et al (2019) Imaging microstructure of the barley  
679 rhizosphere: particle packing and root hair influences. *New Phytologist* 221:1878–  
680 1889
- 681 Kool JB, Parker JC (1987) Development and evaluation of closed-form expressions for  
682 hysteretic soil hydraulic properties. *Water Resour Res* 23:105–114.  
683 <https://doi.org/10.1029/WR023i001p00105>
- 684 Lehmann J, Solomon D, Kinyangi J, et al (2008) Spatial complexity of soil organic  
685 matter forms at nanometre scales. *Nat Geosci* 1:238–242
- 686 Leung AK, Boldrin D, Liang T, et al (2018) Plant age effects on soil infiltration rate  
687 during early plant establishment. *Géotechnique* 68:646–652
- 688 Liu Y, Patko D, de la Mata AL, et al (2025) Microcosm fabrication platform for live  
689 microscopy of plant-soil systems. *Biosyst Eng* 252:105–114
- 690 Loveland P, Webb J (2003) Is there a critical level of organic matter in the agricultural  
691 soils of temperate regions: a review. *Soil Tillage Res* 70:1–18
- 692 Lucas M, Schlüter S, Vogel H-J, Vetterlein D (2019) Roots compact the surrounding  
693 soil depending on the structures they encounter. *Sci Rep* 9:16236
- 694 Lynch JP (2013) Steep, cheap and deep: an ideotype to optimize water and N  
695 acquisition by maize root systems. *Ann Bot* 112:347–357
- 696 Lynch JP, Brown KM (2002) Topsoil foraging - an architectural adaptation of plants to  
697 low phosphorus availability. *Plant Soil* 237:225–237
- 698 Mair A, Dupuy L, Ptashnyk M (2023) Can root systems redistribute soil water to  
699 mitigate the effects of drought? *Field Crops Res* 300:109006.  
700 <https://doi.org/https://doi.org/10.1016/j.fcr.2023.109006>
- 701 Marshall MR, Ballard CE, Frogbrook ZL, et al (2014) The impact of rural land  
702 management changes on soil hydraulic properties and runoff processes: results  
703 from experimental plots in upland UK. *Hydrol Process* 28:2617–2629
- 704 Mualem Y (1976) A new model for predicting the hydraulic conductivity of unsaturated  
705 porous media. *Water Resour Res* 12:513–522.  
706 <https://doi.org/10.1029/WR012i003p00513>
- 707 Nassah H, Er-Raki S, Khabba S, et al (2018) Evaluation and analysis of deep  
708 percolation losses of drip irrigated citrus crops under non-saline and saline  
709 conditions in a semi-arid area. *Biosyst Eng* 165:10–24
- 710 Naveed M, Ahmed MA, Benard P, et al (2019) Surface tension, rheology and  
711 hydrophobicity of rhizodeposits and seed mucilage influence soil water retention  
712 and hysteresis. *Plant Soil* 437:65–81

- 713 Ni JJ, Leung AK, Ng CWW (2019) Modelling effects of root growth and decay on soil  
714 water retention and permeability. *Canadian Geotechnical Journal* 56:1049–1055
- 715 Oberbroeckling KJ, Dunwoody DC, Minter SD, Leddy J (2002) Density of Nafion  
716 exchanged with transition metal complexes and tetramethyl ammonium, ferrous,  
717 and hydrogen ions: commercial and recast films. *Anal Chem* 74:4794–4799
- 718 Ogunmokun FA, Liu Z, Wallach R (2020) The influence of surfactant-application  
719 method on the effectiveness of water-repellent soil remediation. *Geoderma*  
720 362:114081
- 721 R Core Team (2021) R Core Team (2021). R: A language and environment for  
722 statistical computing
- 723 Rawls WJ, Nemes A, Pachepsky YA (2004) Effect of soil organic carbon on soil  
724 hydraulic properties. *Developments in soil science* 30:95–114
- 725 Read DB, Bengough AG, Gregory PJ, et al (2003) Plant roots release phospholipid  
726 surfactants that modify the physical and chemical properties of soil. *New*  
727 *phytologist* 157:315–326
- 728 Read DB, Gregory PJ, Bell AE (1999) Physical properties of axenic maize root  
729 mucilage. *Plant Soil* 211:87–91
- 730 Schmid B, Schindelin J, Cardona A, et al (2010) A high-level 3D visualization API for  
731 Java and ImageJ. *BMC Bioinformatics* 11:274
- 732 Schulz R, Ray N, Zech S, et al (2019) Beyond Kozeny–Carman: predicting the  
733 permeability in porous media. *Transp Porous Media* 130:487–512
- 734 Scott EM, Rattray EAS, Prosser JI, et al (1995) A mathematical model for dispersal of  
735 bacterial inoculants colonizing the wheat rhizosphere. *Soil Biol Biochem* 27:1307–  
736 1318
- 737 Song L, Li JH, Zhou T, Fredlund DG (2017) Experimental study on unsaturated  
738 hydraulic properties of vegetated soil. *Ecol Eng* 103:207–216
- 739 Syms R (2017) Rapid evaporation-driven chemical pre-concentration and separation  
740 on paper. *Biomicrofluidics* 11:
- 741 Unkovich M, Baldock J, Farquharson R (2018) Field measurements of bare soil  
742 evaporation and crop transpiration, and transpiration efficiency, for rainfed grain  
743 crops in Australia—A review. *Agric Water Manag* 205:72–80
- 744 Valat B, Jouany C, Riviere LM (1991) Characterization of the wetting properties of air-  
745 dried peats and composts. *Soil Sci* 152:100–107
- 746 van Genuchten MTh (1980) A Closed-form Equation for Predicting the Hydraulic  
747 Conductivity of Unsaturated Soils. *Soil Science Society of America Journal*  
748 44:892–898. <https://doi.org/10.2136/sssaj1980.03615995004400050002x>
- 749 Vogel T, Zhang R (1996) The HYDRUS Code for Simulating One-Dimensional Water  
750 Flow, Solute Transport, and Heat Movement in Variably-Saturated Media. Version  
751 5.0. <https://doi.org/10.13140/RG.2.1.3456.7525>
- 752 Whalley WR, Riseley B, Leeds-Harrison PB, et al (2005) Structural differences  
753 between bulk and rhizosphere soil. *Eur J Soil Sci* 56:353–360

- 754 Williams A, de Vries FT (2020) Plant root exudation under drought: implications for  
755 ecosystem functioning. *New Phytologist* 225:1899–1905
- 756 Xiao T, Li P, Fei W, Wang J (2024) Effects of vegetation roots on the structure and  
757 hydraulic properties of soils: A perspective review. *Science of The Total*  
758 *Environment* 906:167524
- 759 Zheng W, Zeng S, Bais H, et al (2018) Plant growth-promoting rhizobacteria (PGPR)  
760 reduce evaporation and increase soil water retention. *Water Resour Res* 54:3673–  
761 3687
- 762 Zickenrott IM, Woche SK, Bachmann J, et al (2016) An efficient method for the  
763 collection of root mucilage from different plant species—A case study on the  
764 effect of mucilage on soil water repellency. *Journal of Plant Nutrition and Soil*  
765 *Science* 179:294–302. <https://doi.org/10.1002/jpln.201500511>